8 Electrochemically Formed Film Layers of Importance in Electrocatalysis

B. F. Giannetti, C. M. V. B. Almeida, and S. H. Bonilla

CONTENTS

8.1 Introduction 191
8.2 Classification of Film Models 192
8.2.1 Models Developed for Continuous Films 192
8.2.2 Models for Noncontinuous Films 195
8.2.2.1 Nucleation Theories 195
8.2.2.2 Theories Based on Variable Coverage 196
8.2.2.3 Combined Theories 197
8.3 General Discussion 198
8.4 Diagnostic Parameters' Criteria for the Different Growth Models 198
References 206

8.1 INTRODUCTION

One of the most intensively studied interfaces is the electronic conductor/ionic conductor where the interest is motivated by attempts to prevent corrosion and to improve the catalytic properties of metallic deposition. Both corrosion prevention and catalysis development can be described using an electrochemical and engineering approach, including film formation and growth and its optimization in the cell reactor.

In the case of interdisciplinary areas of study, layers and films with different properties are expected to grow in different ways to fulfill diverse requirements. Thus, the desired characteristics of a film with protective properties against corrosion will differ from those needed to perform as a good electrocatalyst. In this context, it is impossible to think that a unique model would be complete enough to embrace such different films.

As an effort to understand film formation and with the purpose of optimization (predicting, modifying, and/or improving this formation), several models supported by theoretical considerations were developed. In this way, the development of a physical model leads to the derivation of mathematical equations, which enables the development of a theory and comparison with experimental results.

In a general way, the reference point will restrict the way of focusing on the phenomenon and as a consequence it will determine the choice of the variables to be used in it. For the study of film growth and in order to establish a theoretical basis, two different reference points can be equally considered in reality. Figure 8.1 shows two reference points: Observer **B**, denoted with light grey arrows, at a normal position to the metal surface, will be able to describe the process of film growth by choosing variables that will differ, certainly, from those from Observer **A**, placed parallel to the surface, denoted with dark grey arrows.

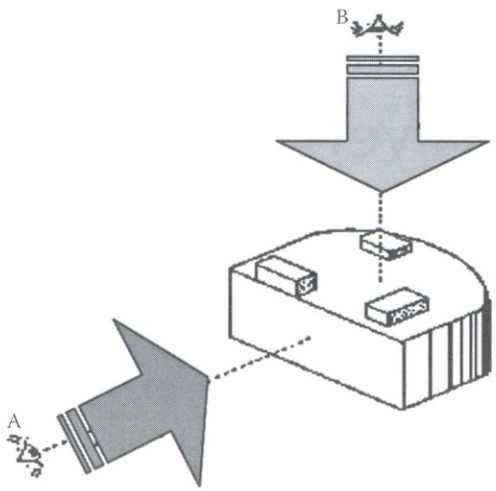

FIGURE 8.1 The aspect of film growth with the point of view of different imaginary observers: A (dark grey) along a parallel direction of movement and B (light grey) through a perpendicular position to the surface.

The rate of metal or metallic oxide nuclei formation during charge transfer, or the temporal variation of the degree of surface coverage will be useful to follow, describe and quantify the film formation for Observer B. On the other hand, Observer A, with a different perception of the same process, will be able to describe film growth in terms, for example, of ion transport through (or to) the substrate and/or the electrolyte. As a consequence, different growth models can be projected, making the selection of the most plausible model very difficult. The singular use of mathematical considerations to support the selection of the most satisfactory model should be avoided, and special emphasis should be put to verify the physical connotation of the parameters.

We are going to present a review of the main models of electrochemically formed films with the purpose of giving an initial reference to the subject and then illustrate the selection procedure to choose the most suitable model with an emphasis on the physical meaning of the determining variables.

8.2 CLASSIFICATION OF FILM MODELS

In general, films can be grouped as continuous and noncontinuous according to the morphology of the obtained surface. The former assumes that the metal surface is completely covered by the film. Continuous films form in systems where the mass transport of ion species toward the solution is hindered. On the other hand, systems in which the transport of ions to the solution is allowed give a noncontinuous film, that is, first a vacancy substrate site is defined, which in the progress of the growth, can lead to an irregular or porous film.

8.2.1 Models Developed for Continuous Films

According to the basic statement of the models we are going to summarize, the metal is conceived as a network of cations immersed in a "cloud" of free electrons in a crystalline structure. The transport of the ions controls the growth of the new phase (Figure 8.2). The ionic transport will depend on the nature of the system and on experimental conditions, such as temperature, local electric field, local concentration excess, etc. To better understand the continuous-film models, the main ionic transport mechanisms in crystalline solids are presented [1] as follows.

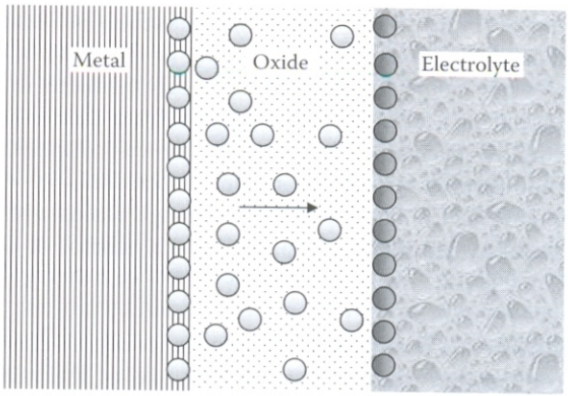

FIGURE 8.2 The growth of a new oxide phase on the metal with the process controlled by the mass transport of cations, symbolized as ○ toward the solution, where the oxygen anions are symbolized as ●.

1. *Interstitial mechanism* (Figure 8.3A). The displacement of metal atoms takes place from one interstitial site to the other without permanently displacing the matrix atoms in the crystal cell. The distortion caused by the movement of the matrix atoms to allow "the jump" constitutes the energy barrier that must be surmounted. This mechanism is frequently used to describe film formation on metal alloys when metal atoms normally occupy interstitial positions.
2. *Vacancy mechanism* (Figure 8.3B). The movement of adjacent atoms occurs to an unoccupied site (vacancy) because of the surface energy difference between them. The lattice distortion caused by the movement of a neighboring atom through the vacancy is lower than that predicted by the interstitial mechanism. This mechanism is well known and is often used to describe film formation on metals, metal alloys, ionic compounds, and oxides.

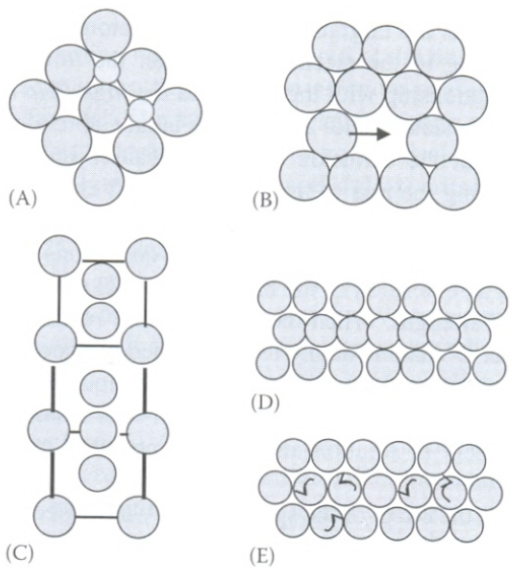

FIGURE 8.3 Simplified schemes for the main mechanisms of transport of atoms in solids. (A) Interstitial; (B) vacancy; (C) interstitially; (D) crowed-ion; (E) ring mechanisms.

3. *Interstitially mechanism* (Figure 8.3C). The atoms placed at the interstitial sites can move, pushing the nearest neighboring atom and displacing it. This kind of mechanism occurs in "metallic solutions" when solute atoms are the same size as matrix ones. The displacement of several atoms placed in a close-packed direction from their equilibrium position by means of an interstitially mechanism is called the *crowd-ion mechanism* (Figure 8.3D). This kind of distortion spreads out only along one dimension.
4. *Ring mechanism* (Figure 8.3E). The atoms can exchange places with their neighbors, and the deformation caused by the rotation depends on the number of atoms that are able to rotate.

The electrochemical growth of a continuous and homogeneous film can be well thought-out as a result of the migration of metallic cations by means of one of the above-mentioned transport processes. It is worthy to note that the dislocation of ions breeds defects (vacancies, interstitial ions, etc.). Hence, either the dislocation of defects or the migration of atoms can be used to describe the transport process [1]. Mathematical details are found in the cited references and also in the reviews [2,3].

Lanyon and Trapnell [4] and, later, Green [5] and Law [6] described the initial stages of metal oxidation by using the ring mechanism (known as "place exchange"). According to these authors, an oxygen atom adsorbed on the metal surface (M–M–O) can rotate, changing places with an adjacent metal atom (M–O–M). This process, successively repeated, would increase the thickness of the oxide film. Sato and Cohen [7] developed mathematical equations for the model when stationary electrochemical techniques were applied to generate the film. The authors assumed that all the rotations were simultaneous and that the activation energy for the place exchange increased linearly with film thickness. For increasing thickness, the activation energy would reach values excessively high, and another growth mechanism would become dominant, for example, the interstitial mechanism. Asakura and Nobe [8] solved the mathematical equations for potentiodynamic conditions, resulting in a linear relationship between the current intensity and the potential scan rate.

The model developed by Verwey [9] assumed that film growth occurred through an interstitial mechanism where the distortion of the lattice was the same for all the position changes; thus, the energy barrier is symmetric and periodic. The presence of a uniform electric field, however, could diminish the barrier promoting the migration of ions in a given direction. The rate-determining step of the process was considered as the migration of interstitial atoms inside the lattice. Two limiting cases were discussed according to the electric field value: the *low-field model*, where the total current presents an ohmic relationship with the field, and the *high-field model*, where the current is an exponential function of the electric field. Some years later, Cabrera and Mott [10], using similar considerations, considered that the diffusion of defects causes an accumulation of ions at the metal/film interface determining the rate of the process. The Verwey model [9] and the model of Cabrera and Mott [10] were developed for steady-state stationary electrochemical conditions. Mathematical expressions developed for potentiodynamic conditions are grouped elsewhere [11].

Lohrengel [12] proposed an extension of the high-field model where the concentration of defects varies with the electric field strength. When the concentration reaches a constant value, the high-field equations may be valid. D'Alkaine et al. [13] developed a model where migration is the main type of transport, applied for both stationary [13,14] and potentiodynamic [14,15] conditions of film growth. In this case, it was assumed that the movement of ions inside the film presents characteristics similar to their movement in solution and that the potential gradient across the film obeys a linear relationship.

In all the previous models, the effect of the space charge was neglected. Dewald [16] was the first to take into account the effect of the space charge. Moreover, Young [17] completed an extension of the theory by assuming a uniform space charge within the film; however, the equations resulting from Dewald's theory [16] do not relate current density with the electric potential. The hypothesis of Verwey, Cabrera, and Mott corresponds to limiting situations of the general case.

Bean et al. [18] considered that mobile interstitial ions are created within the film when the metal ions move out of their normal sites, leaving vacancies. The creation of mobile ions is a field-dependent process, so a fixed concentration of interstitial ions exists at characteristic field strength. This kind of transport occurs frequently in amorphous oxides.

Chao et al. [19] proposed a model that explains the growth of a film under steady-state conditions. It was considered that the passive film contains a high concentration of no recombining point defects. Metal/film and film/solution interfaces were assumed to be at electrochemical equilibrium. This theory successfully accounts for the linear dependencies of both the steady-state film thickness and the logarithm of the passive current on the applied voltage.

Bojinov et al. [20] considered the retarding, as well as the enhancing, effect of the defect migration within the film due to the excess of charge in the metal/film or the film/electrolyte interfaces. A high electric field that assisted the migration of defects was assumed for film growth. The model was developed considering electrochemical impedance measurements. The decrease of the electric field within the film as a consequence of the accumulation of interfacial charges is considered in the equations.

Several models were developed to describe the growth of continuous films. It is worthy of attention that those theories are based on the point of view of Observer A, placed parallel to electrode surface (Figure 8.1).

8.2.2 Models for Noncontinuous Films

Models that describe the growth of noncontinuous films use the point of view of Observer B (Figure 8.1) and can be classified into three main groups:

1. *Nucleation theories*. Nuclei are generated onto the electrode surface and grow with a given orientation and shape.
2. *Theories of variable coverage*. The surface coverage is the main parameter for the description of the film-formation kinetics.
3. *Combined theories*. Models that combine aspects of both of the previous theories are able to describe the formation of the film.

8.2.2.1 Nucleation Theories

The first scientific reports regarding nucleation appeared at the beginning of the twentieth century [21–24]. According to these theories, the formation of micro-phases, nuclei, takes place at active sites that are energetically favored. The study of nuclei formation and growth requires the use of techniques that enable very fast recording of the electrochemical response in order to register the first instants of film formation. For this reason, successful experimental results were only accomplished after the 1950s due to progress in electronics.

Fleishmann and Thirsk [25–27] derived analytical expressions for a nucleation model under potentiostatic conditions relating current with time (chronoamperometric plots). They assumed that there are N_0 active sites available on the substrate and that N nuclei are generated. Both parameters considered there were related through an exponential expression, which involved time and a factor depending on the overpotential. Two limiting cases of nucleation rates were described. The assumption of a large dependence on overpotential led to an instantaneous coverage of all the active sites (*instantaneous nucleation*). On the other hand, a slight dependence on the overpotential led to a lower nucleation rate (*progressive nucleation*). The nucleation rate also depends on the surface area occupied by the growing nuclei; thus, nuclei can grow without area changes, and this process is called one-dimensional growth. Bidimensional growth occurs, on the other hand, when lateral area increases and, in the case of three-dimensional growth, the whole superficial area of the nuclei is affected during growth. In addition, the geometry of the nucleus determines the electrical current expression.

When contact between the nuclei is neglected during growth, an independent type of growth is assumed. This assumption may be true in the early stages of growth; however, as radial growth proceeds, the occupied area of a growing nucleus will be limited by the presence of neighboring nuclei. As a consequence, overlapping of the nuclei can occur. Bewick et al. [28] applied Avrami's theorem [29] to estimate the overlapped area.

Although the latter models assumed that the slowest step involves the incorporation of species at the periphery of expanding nucleus, other nucleation models proposed that mass transfer in solution controlled the new phase growth [30–32].

Scharifker [33] considered that two processes interact in the film formation kinetics: the activation and the deactivation of sites on the substrate. Thus, the deactivation, caused by the development of a hemispherical diffusion field centralized at each nucleus, inhibits film growth in the neighborhood of the diffusion centers.

Barradas and Bosco [34] presented three novel models of two-dimensional nucleation. They involve the coupling of nucleation with diffusion in the electrolyte, with and without additional metal dissolution from the electrode surface.

The effect of potentiodynamic perturbations was only considered in the early seventies [35–39]. The delay was possibly due to the difficulty in dealing with the mathematical expressions, in which the nucleation rate depends on the applied overpotential, which varies with time. For this reason, limiting conditions of low potential scan rate ($v \rightarrow 0$) and high potential scan rates ($v \rightarrow \infty$) were considered. The limiting situations were called, rather arbitrarily, "reversible" and "irreversible" [39], and the model describes a nucleation-growth-overlap process in two steps: instantaneous and progressive. A scheme of the nucleation-growth-overlap model is shown in Figure 8.4. This model can be applied either for the study of the formation of a new phase (Figure 8.4A) or substrate dissolution (Figure 8.4B) [36,40].

8.2.2.2 Theories Based on Variable Coverage

Among the models developed for steady-state stationary conditions, the time-dependent surface coverage can be the real description of the growth of the new phase. Ogura [41] assumed that the film was generated from the active dissolution of the metal. The author derived expressions in order to determine Tafel coefficients corresponding to the following rate-determining steps: metal dissolution, film formation, and film development for the cases of high and low overpotentials. On the other hand, Ebersbach et al. [42] proposed a mechanism where the film growth would inhibit the metal dissolution (passivation). The kinetics of passivation is then explained as a competition between the formation of the oxide film and metal dissolution.

In 1931, Müller [43] explained the formation of a porous, insoluble, and poor conducting film by means of a simplified model based on potentiostatic experiments. In this way, it was considered that film formation occurs through the following simple, fast reaction:

$$M(s) + X^- \leftrightarrow MX(s) + ne^- \qquad (I)$$

FIGURE 8.4 Schematic illustration of film formation (A) and dissolution (B) on the substrate according to the nucleation-growth-overlap model.

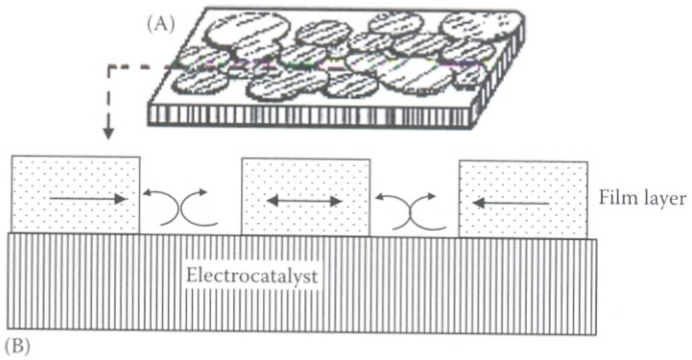

FIGURE 8.5 Passive film growth according to Müller's model. (A) Observer's B view and (B) Observer's A view.

where MX are solid species able to form nuclei, subsequently spreading laterally and finally generating a porous film. As the degree of coverage increases, the metallic area exposed to dissolution decreases, and the reaction rate would be limited by the resistance of the solution in the pores of the film (Figure 8.5). When the film covers approximately 99% of the surface, the resistance reaches its maximum value, inhibiting the film formation.

Calandra et al. [44] adapted Müller's model to potentiodynamic conditions. Mac Donald [45] corrected a typographical error found in the mathematical expressions in the article. Devilliers et al. [46] developed a general model for the formation of low-conductivity films, considering a process controlled by the solution resistance in the pores of the film. The authors simulated the potentiodynamic curves for the following particular cases: constant film thickness (bidimensional growth), three-dimensional growth, and a decomposition/dissolution process coupled to the electrochemical reaction. The potentiodynamic curves simulated for constant thickness are identical to those obtained by Calandra et al. [44].

Srinivasan and Gileadi [47] described the formation of a new phase under potentiodynamic conditions in terms of an adsorption process. The validity of the Langmuir isotherm was assumed for the following adsorption process:

$$A^- \leftrightarrow A_{ads} + e^- \qquad \text{(II)}$$

Two situations were considered in the derivation of the equations: the *quasi-equilibrium* and the *irreversibility* of the reaction of the formation of adsorbed species.

Several authors [39,47–53] considered a more realistic hypothesis taking into account the long-range interactions between the adsorbed species, that is, the verification of the Frumkin isotherm. The mathematical relations, however, were obtained only for reversible processes [39,51,52].

8.2.2.3 Combined Theories

The description of film formation in terms of the combination of both nucleation and adsorption processes under potentiostatic [54,55] and potentiodynamic [39] conditions was later adopted. Mathematical simulations of the potentiodynamic curves [39] indicated that only one peak is recorded when the sites on the substrate are the same for both nucleation and adsorption (competitive process); however, when the surface sites for both processes are different (noncompetitive process), the potentiodynamic curves exhibit two current peaks.

8.3 GENERAL DISCUSSION

As it was mentioned in Section 8.1, an experiment is included in order to illustrate the selection procedure. Each model was developed for specific experimental conditions. Sometimes, a description can be modified, extended, and corrected in order to cover other experimental conditions. Thus, a model initially developed with the purpose of describing a film formed under potentiostatic conditions can be adapted, via mathematical derivations, to potentiodynamic conditions. In the present experiment, the film considered was generated under potentiodynamic conditions by the use of voltammetric techniques. As a consequence, only the models developed for potentiodynamic conditions were considered [56–58].

8.4 DIAGNOSTIC PARAMETERS' CRITERIA FOR THE DIFFERENT GROWTH MODELS

A mechanically polished tin disk immersed in 0.5 M citric acid was prepared following the procedure described in the literature [59]. Because high-scan-rate voltammetric curves were recorded, a calomel reference electrode is not recommended because of its slow response [60]. The reversible hydrogen electrode (RHE) was used as the reference electrode at 25°C. The required materials and reagents are a three-compartment electrochemical cell with a platinized platinum auxiliary electrode and a 0.5 M (pH = 1.8) citric acid solution prepared with triple-distilled water.

In order to obtain reproducible results, the working electrode must be pretreated as explained in the following text: the electrode used herein was polished with 600 emery paper and alumina suspension (0.3–0.2 μm granularity), washed in distilled water, immersed in a previously deaerated solution, and cathodically polarized at −0.9 V for 5 min. The latter step is important to reduce the oxide layer formed during polishing; however, polarization times longer than this period have to be avoided, otherwise hydride formation and metal lattice reconstruction turn up as a consequence of molecular hydrogen inclusion.

Figure 8.6 shows the voltammetric profile run at 0.1 V s^{-1} for polycrystalline tin in citric acid as reported before [61–65] between −0.9 and 3.0 V with the following main features:

1. Hydrogen evolution occurs at potentials lower than −0.5 V.
2. An anodic current, A_1, appears near 0 V.
3. A low stationary current (passive state) is observed after the anodic peak, until approximately 3.0 V.

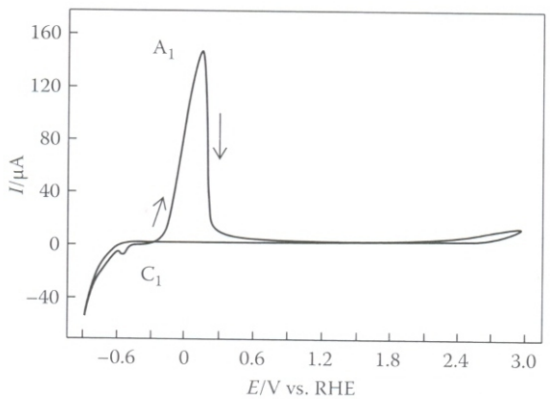

FIGURE 8.6 Current versus potential profile for polycrystalline tin in 0.5 M citric acid (pH = 1.8) run at 0.1 V s^{-1} between –0.9 and 3.0 V. $A = 0.8$ mm^2.

4. Oxygen evolution occurs above 3.0 V, indicative of the conductivity of the formed passive film.
5. A cathodic current peak, C_I, appears during the potential scan toward negative potentials, around the potential at which hydrogen evolution begins, similarly to other non-noble metals in acid solution.

The significantly higher anodic charge and the sudden current fall immediately after the peak are evidence for a net oxidation process with little redeposition on the electrode surface.

Accordingly, the oxidation current can be written as the sum of two contributions:

$$I = I_D + I_F \tag{8.1}$$

with I_D being the current related to the active dissolution of the metal and I_F being the current related to the film formation.

The first step considered in the selection procedure corresponds to the verification of the mathematical relationships resulting from the models. For this purpose, the experimental data is analyzed according to the mathematical relationships of the most suitable theoretical models. Table 8.1 will be very useful as it collects the mathematical relationships satisfied by models developed for potentiodynamic conditions.

Obviously, experimental data should verify all the mathematical expressions of the proposed model as a necessary condition to satisfy. Besides, it is not rare that several model expressions present linear relations involving the same variables. In these cases, it is risky to choose a model based solely on mathematical criteria. In these cases, the calculation of the model's parameters from the experimental data is a necessary condition to assume or to reject a model. If the values calculated from experimental data do not present physical meaning, the model is not applicable.

Graphs corresponding to peak current (I_p) versus v as well as peak potential (E_p) versus log v for peak A_I (Figures 8.7 and 8.8) show three regions, labeled A, B, and C. Region A is comprised of the 0–0.2 V s^{-1} domain, followed by region B that extends up to 7 V s^{-1}. The last, region C, falls between 7 and 22 V s^{-1}. The linear dependence of I_p versus v in region A (Figure 8.7), together with the constant behavior observed in the E_p versus log v plot (Figure 8.8), could support the Srinivasan–Gileadi model [47] (Table 8.1).

According to this model, a film formation controlled by a quasi-reversible adsorption seems to be suitable to describe the process occurring in the scan rate domain of region A. On the other hand,

TABLE 8.1
Diagnostic Parameters' Criteria for the Different Growth Models: Nucleation-Growth-Overlap (I) [39]; Müller–Calandra (II) [43,44]; and Srinivasan–Gileadi (III) [47] under Potentiodynamic Conditions

Parameter	(I) ($v \to 0$)	(I) ($v \to \infty$)	(II)	(III) Quasi-Reversible	(III) Irreversible
I_p/v	—	Constant	—	Constant	Constant
$I_p/v^{1/2}$	—	Constant	—	Constant	Constant
E_p/v	—	—	—	No	—
$E_p/v^{1/2}$	Constant	—	Constant	Varies on v	—
$E_p/\log v$	—	Constant $= 59/\alpha n$ mV	—	$E_p(v) =$ constant	Constant $= 0.086T/n$ mV K^{-1}
$E_{1/2}/v$	Constant	Constant $= 31/\alpha n$ mV	—	—	—
θ_p	—	0.63	0.999	0.5	0.63

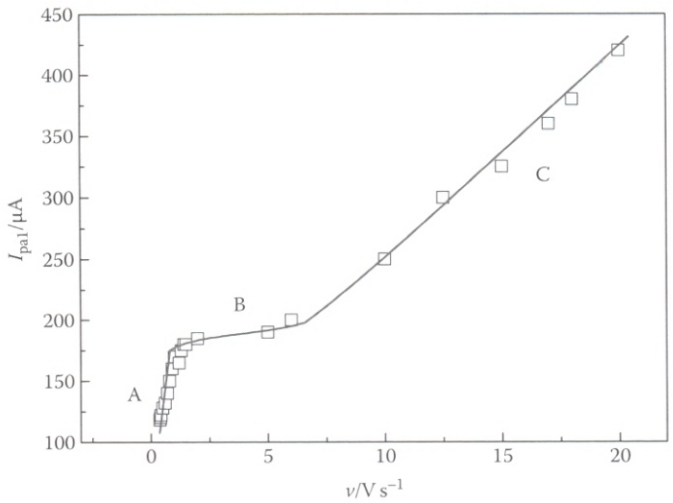

FIGURE 8.7 Current peak (I_p) versus log scan rate (log v) for peak a_I in the case of Figure 8.6.

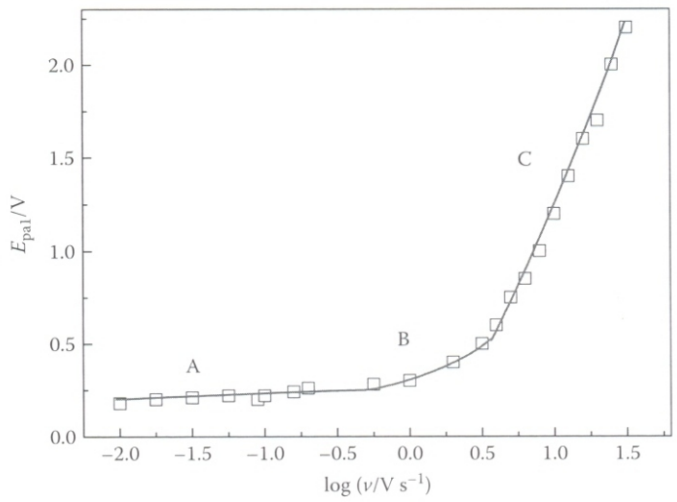

FIGURE 8.8 Potential peak (E_{pa1}) for peak A_I versus scan rate (v) in the case of Figure 8.6.

region C presents a linear behavior for both peak potential and current. Also, the Srinivasan–Gileadi model [47] (but in its limited application for an irreversible adsorption) seems reasonable (at least from a mathematical standpoint) to explain the film-formation process under region C conditions.

Two of the relationships compiled in Table 8.1 (corresponding to two applications related to the Srinivasan–Gileadi model [47]) reflect the mathematical dependence shown in the graphics; thus, the film formation process could be controlled by quasi-reversible adsorption in region A and by irreversible adsorption in region C. It is, therefore, advisable to examine the physicochemical processes involved, that is, to verify if the theoretical model is consistent with the observed phenomenon. In this way, complementary results are obtained.

The variation of the total anodic and cathodic charges with scan rate (Figure 8.9) indicates that for $v < 0.2\ V\ s^{-1}$ (region A), the current contribution corresponding to dissolution (I_D) is significantly higher than that corresponding to film formation (I_F). From the experiments for stirred and

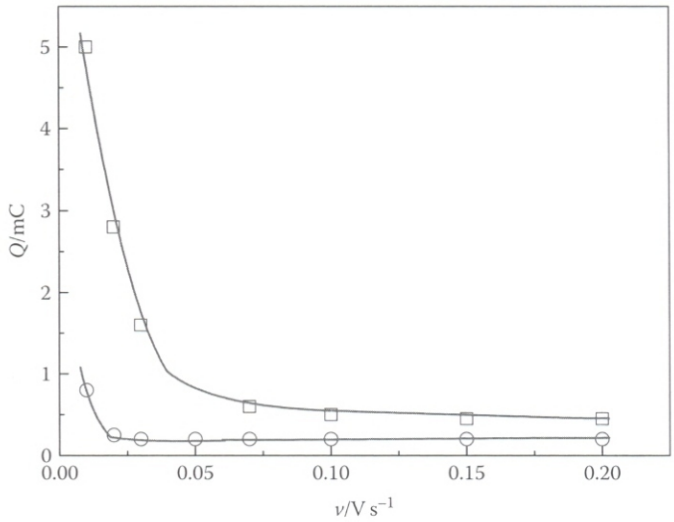

FIGURE 8.9 Absolute charge (Q) versus v for the (○) anodic and (□) cathodic components in the cyclic voltammetric profile of Figure 8.6.

unstirred solutions, it can be stated that at relatively low scan rates the hydrodynamic perturbation affects the peak A_I profile. On the other hand, it can be concluded that under high–scan rate conditions, transport is not the controlling step of anodic process and no changes are proven in the voltammetric profile.

In view of these last results, the 0.2 V $s^{-1} < v < 7$ V s^{-1} region (region B in Figure 8.7) could represent a transition between regions A and C. A review of these last results shows that the suitable model tested by the mathematical correspondence with experimental results for region A does not reflect the real performance of the system because current contributions from dissolution are neglected. As a consequence, the model was discarded.

For region C, the lack of a physical meaning for the parameters calculated using the proposed model was evident, resulting in a need to disregard of the proposed model. To discuss the discrepancies between the theoretical and the calculated parameters, the following equations (and corresponding to the employed models) will be useful.

The slope, $dE_p/d\log v$, of the straight line in Figure 8.8 (region C) equals 1.55. Assuming the validity of the Srinivasan–Gileadi model and considering a symmetry factor of 0.5, the number of electrons results in $n = 0.03$ from (Equation 8.6), a number without physical meaning. Thus, it can be concluded that, despite the linearity observed in region C, the Srinivasan–Gileadi model is not applicable to the studied system.

In order to continue with the selection procedure, another mathematical relationship presented in Table 8.1 was tested. Figures 8.10 and 8.11 show that both I_p and E_p vary linearly with the square root of v, only for $v > 7$ V s^{-1}. The diagnostic criteria in Table 8.1 indicate that the film formation can be described by the dissolution–precipitation model proposed by Müller and Callandra [43,44]. According to this model, the resistance remains low until the film covers 99% of the surface; therefore, it is reasonable to assume that the anodic current reaches its maximum when the entire surface is practically covered. As the total anodic current is the combined result of two contributions, namely, dissolution and formation of the film, the degree of coverage cannot be graphically evaluated from the voltammograms. Assuming that the film consists basically of SnO_2 [66], and that $\rho = 6$ g cm^{-3}, $\chi = 6 \times 10^{-3}$ S m^{-1}, and $S = 8 \times 10^{-3}$ cm^2, and that the value of $dI_p/dv^{1/2}$ calculated from Figure 8.10 is 84.6×10^{-6} A $(V\ s^{-1})^{-1/2}$, the coverage is $\theta = 0.9989$. The expressions for the peak current and potential are defined in the original article [44].

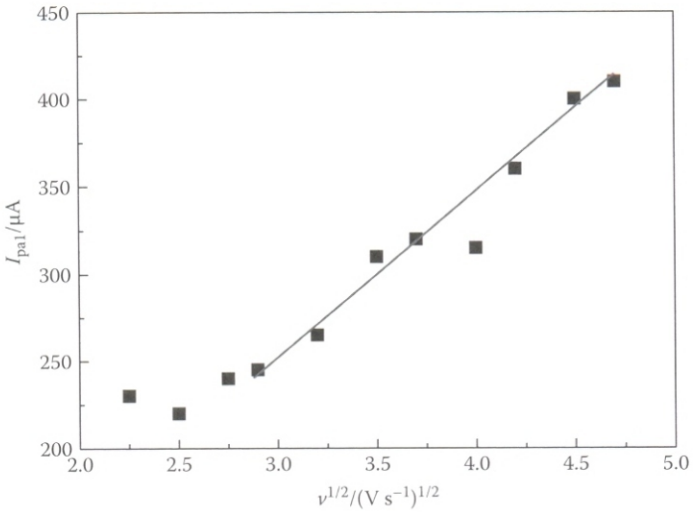

FIGURE 8.10 I_{pa1} versus $\nu^{1/2}$ plot for peak A_I at $\nu > 8$ V s^{-1}. Data from Figure 8.6.

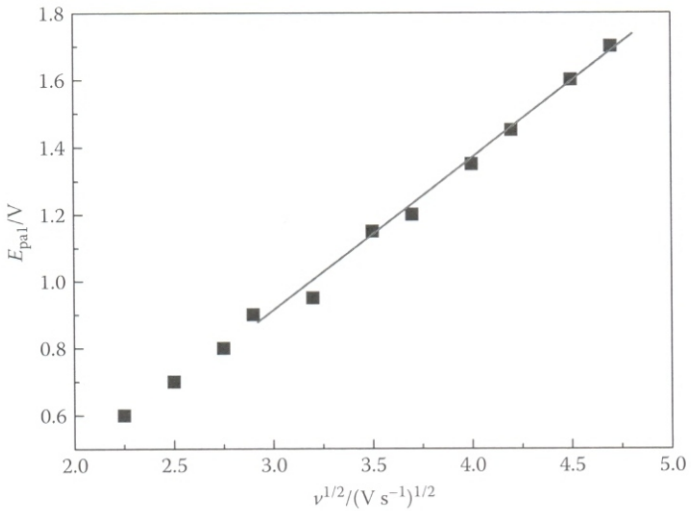

FIGURE 8.11 E_{pa1} versus $\nu^{1/2}$ plot for peak A_I at $\nu > 8$ V s^{-1}. Data from Figure 8.6.

In the Müller–Calandra model for noncontinuous growth on a porous surface, the limiting condition in a potentiodynamic experiment is the resistance of the solution within the pores. The following parameters rise up for a 0.999 of surface coverage (θ) for the growth of a *PM* (molecular weight) formation:

$$I_p = \sqrt{\frac{nF\rho\chi}{PM}} S(1-\theta)\nu^{1/2} \tag{8.2}$$

$$E_p = \sqrt{\frac{nF\rho\chi}{PM}} \left[\frac{\delta}{\chi} + R_o S(1-\theta)\right] \nu^{1/2} \tag{8.3}$$

where
- δ is the thickness of the film
- ρ is the solution density
- χ is the conductivity of the solution in the pores
- S is the real surface area of the electrode
- R_o is the total resistance

Besides, two cases can be found for the Srinivasan–Gileadi model using variable conditions of the surface coverage under potentiodynamic experiments. In the case of a reversible adsorption and for the standard condition $\theta = 0.5$

$$I_p = \frac{\sigma F}{4RT} v \tag{8.4}$$

$$E_p = -\frac{RT}{F} \ln K \tag{8.5}$$

where K is the equilibrium constant of the film formation process. On the other hand, in the case of the irreversible adsorption, the standard condition of $\theta = 0.63$

$$I_p = \frac{(1-\theta)\beta n \sigma F}{4RT} v \tag{8.6}$$

$$E_p = \frac{RT}{\beta nF} \ln\left(\frac{\beta nF\sigma}{k^o RT}\right) + \left(\frac{RT}{\beta nF}\right) \ln v \tag{8.7}$$

where
- σ is the charge density required to form a monolayer of the film
- β is the symmetry factor
- k^o is the specific rate constant for the forward process (film formation)

The nucleation theories for potentiodynamic conditions [44] lead mainly an instantaneous or progressive nucleation also for reversible and irreversible limiting conditions. The following dependences of I_p, E_p, and $\Delta E_{1/2}$ with v can be obtained for four limiting cases.

1. Instantaneous nucleation for a reversible process

$$I_p = 8.94S\left(\frac{N_T}{N_o}\right)^{1/4} \sigma \sqrt{nk_g v} \tag{8.8}$$

$$E_p = E^o + \left(\frac{0.1584}{\sqrt{nk_g}}\right)\left(\frac{N_T}{N_o}\right)^{1/4} v^{1/2} \tag{8.9}$$

$$\Delta E_{1/2} = \left(\frac{0.2060}{k_g\sqrt{n}}\right)\left(\frac{N_T}{N_o}\right)^{1/4} v \tag{8.10}$$

where
- N_T is the total number of sites on the substrate (number cm^{-2})
- N_o is the number of active sites on the substrate (number cm^{-2})

2. Instantaneous nucleation for an irreversible process

$$I_p = 28.63S\sigma\alpha nv \tag{8.11}$$

$$E_p = E^{o'} - \frac{0.7936}{\alpha n} + \frac{0.02959}{\alpha n}\log\left[\left(\frac{N_T}{N_o}\right)\left(\frac{nv}{k_g}\right)^2\right] \tag{8.12}$$

$$\Delta E_{1/2} = \left(\frac{0.0314}{\alpha n}\right) \tag{8.13}$$

3. Progressive nucleation for a reversible process

$$I_p = 0.3679K^2S\sigma v/a \tag{8.14}$$

$$E_p = E^{o'} + \frac{a}{K} \tag{8.15}$$

$$\Delta E_{1/2} \to 0 \tag{8.16}$$

where a is the potential dependent nucleation parameter in volts and K is

$$K = -9.04 + 2.303\log\left[\left(\frac{N_o}{N_T}\right)\frac{k_N k_g^2}{n^2a^3v^3}\right] \tag{8.17}$$

4. Progressive nucleation for an irreversible process

$$I_p = 28.63S\sigma\alpha nv \tag{8.18}$$

$$E_p = E^{o'} + \frac{0.0147}{\alpha n} + \frac{0.02959}{\alpha n}\log\left[\left(\frac{\alpha nv}{k_N}\right)\left(\frac{\alpha nv}{k_g}\right)^2\right] \tag{8.19}$$

$$\Delta E_{1/2} = \left(\frac{0.0314}{n}\right) \tag{8.20}$$

where

k_N is the nucleation velocity (s^{-1})

k_g is the growth rate of the nuclei (s^{-1})

The graph of I_p versus $v^{1/2}$ (Figure 8.10) gives a straight line that does not pass through the origin as expected from the mathematical expression derived for the model [43,44]. The nonzero intercept results from the presence of dissolution current, not considered in the model, where only the actions of I_F versus v were taken into account.

Scanning electron microscopy results showed that the surface aspect, after a potential sweep from –0.9 to 2.0 V at 0.1 V s^{-1} and a holding at the last potential for 10 min, supported the idea that the film is formed by precipitation (noncontiguous aspect) and presented a porous aspect (see micrograph in Ref. [62]).

The complete diagnostic criteria related to the model was satisfied and considering that other experimental evidence also support it, it is reasonable to conclude that at high scan rates (region C) the film growth is controlled by pore resistance, as stated by the Müller and Calandra model [43,44].

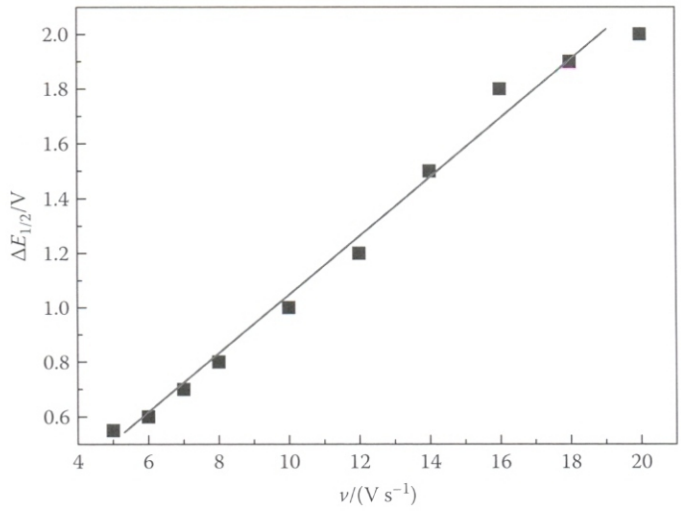

FIGURE 8.12 $\Delta E_{1/2}$ versus v plot for peak A_I at $v > 8$ V s^{-1}. Data from Figure 8.6.

On the other hand, it was verified that the half-peak width $\Delta E_{1/2}$ varies linearly with scan rate (Figure 8.12). This linear relationship together with those observed in Figures 8.10 and 8.11 are predicted by the nucleation-growth model for potentiodynamic conditions [39] when the nucleation process is fast and irreversible.

The instantaneous nucleation-growth-precipitation model [39] assumes that the film is formed directly on the substrate, without previous dissolution; however, it was observed that active dissolution of the metal occurs. Therefore, Equations 8.11 through 8.13 were examined and rewritten considering metal dissolution, that is, terms corresponding to dissolution were added to the mathematical expressions:

$$I_p = I'_p + 28.63(\alpha n)\,\sigma v \tag{8.21}$$

where

α is the charge transfer coefficient (linear combination of β)

σ is the total surface charge density

$$E_p = E'_p + \left\{E^{o'} - 0.7936/(\alpha n) + [0.02959/(\alpha n)]\log\left[(N_T/N_o)(nv/k_g)^2\right]\right\} \tag{8.22}$$

$$\Delta E_{1/2} = \Delta E'_{1/2} + 0.0314/(\alpha n) \tag{8.23}$$

And now rearranging the equations and dividing (8.21) by (8.22) and a part (8.22) with (8.23) we can obtain the following equation:

$$\frac{\left(I_p - I'_p\right)}{\left(E_p - E'_p\right)} = 56.44\left(\frac{N_o}{N_T}\right)^{1/2} nS\sigma k_g \tag{8.24}$$

$$\left(\Delta E_{1/2} - \Delta E'_{1/2}\right)\left(E_p - E'_p\right) = \frac{1.3v^{1/2}}{k_g^{1/2}} \tag{8.25}$$

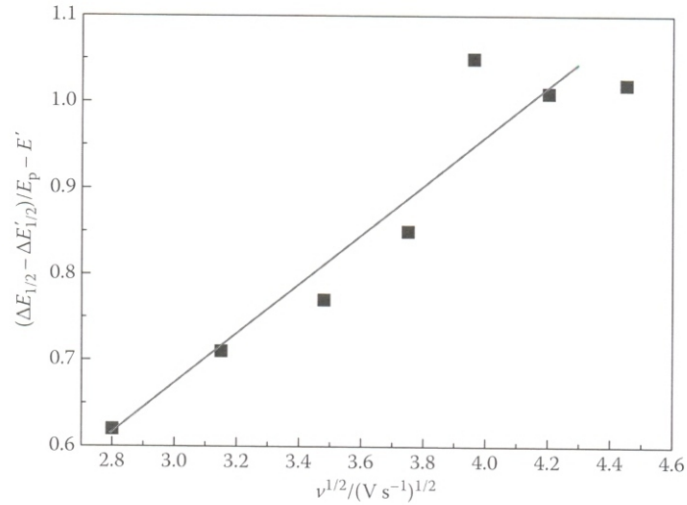

FIGURE 8.13 $\Delta E_{1/2} - \Delta E'_{1/2}$ versus $v^{1/2}$ plot for peak A_1 at $v > 8$ V s^{-1}. Data from Figure 8.6.

The value of k_g calculated using (8.25) from the slope of the line in Figure 8.13 (0.24 s$^{1/2}$) is 29 s^{-1}. Because the growth rate depends on the nature of the system and on the characteristics of the applied perturbation, it is not possible to check the value of k_g with values given in the literature. The value of k_g is useful, however, for the evaluation of the number of active sites on the substrate, N_0. With this value, it is possible to verify the suitability of the model, as it is easily comparable with other system values.

The mean value of $\left(I_p - I'_p\right) \Big/ \left(E_p - E'_p\right)$, 1.8×10^{-4} s, obtained from Figure 8.13, and (8.24), gives $k_g = 29$ s^{-1}, with $S = 8 \times 10^{-3}$ cm^{-2}. Assuming that the film is formed, basically, by SnO_2 (then, $n = 4$ and $\sigma = 0.6$ mC cm^{-2} [66]), the ratio between the number of active sites and the total number of sites, N_0/N_T, equals 3.2×10^{-5}.

The total number of sites, $N_T = 9.4 \times 10^{14}$ sites cm^{-2}, was calculated by [39]

$$N_T = \frac{\sigma N_A}{nF} \tag{8.26}$$

The number of sites participating in the formation of SnO_2 is $N_0 = 3.0 \times 10^{10}$ cm^{-2}. This value is similar to those usually found for active sites in the case of metals [67]. As the diagnostic criteria for the instantaneous nucleation-growth-overlap model was fulfilled and physicochemical data obtained for N_0 is physically plausible, we may conclude that instant nucleation with lateral growth of the film occurs. Taking into account that the atomic density of the substrate is of the order of 10^{15} cm^2 [67], we conclude that the density of the active sites on the surface can severely limit the nucleation process.

The fact that the experimental data fit both models, the dissolution–precipitation and the instantaneous nucleation-growth-overlap models, confirms the assertion made at the beginning of this chapter, that is, some models are complementary to each other.

REFERENCES

1. P. G. Shewmon, *Diffusion in Solids*, McGraw-Hill: New York (1963), Chapter 2.
2. M. J. Dignam, in *Comprehensive Treatise of Electrochemistry* (J. M. Bockris, B. E. Conway, E. Yeager, R. E. White, Eds.), Plenum Press: New York (1981), Chapter 5, p. 4.
3. D. A. Vermilyea, in *Advances in Electrochemistry and Electrochemical Engineering* (P. Delahay, C. W. Tobias, Eds.), Interscience: New York (1963), Vol. 3, Chapter 4.

4. A. H. Lanyon and B. M. W. Trapnell, *Proc. Roy. Soc.* **227A** (1955) 387.
5. M. Green, *Prog. Semicond.* **4** (1960) 37.
6. J. T. Law, *J. Phys. Chem. Solids* **4** (1958) 91.
7. N. Sato and M. Cohem, *J. Electrochem. Soc.* **111** (1964) 512.
8. S. Asakura and K. Nobe, *J. Electrochem. Soc.* **118** (1971) 536.
9. E. J. W. Verwey, *Physica* **2** (1935) 1059.
10. N. Cabrera and N. F. Mott, *Rep. Prog. Phys.* **12** (1948) 63.
11. A. Wieckowski and E. Ghali, *Electrochim. Acta* **30** (1985) 1423.
12. M. M. Lohrengel, *Mat. Sci. Eng.* **R11** (1993) 243.
13. C. V. D'Alkaine and M. N. Boucherit, *J. Electrochem. Soc.* **144** (1997) 1331.
14. C. V. D'Alkaine, L. M. M. De Souza, and F. C. Nart, *Corros. Sci.* **34** (1993) 129.
15. C. V. D'Alkaine and M. A. Santanna, *J. Electroanal. Chem.* **457** (1998) 13.
16. J. F. Dewald, *J. Electrochem. Soc.* **102** (1955) 1.
17. L. Young, *Can. J. Chem.* **37** (1959) 276.
18. C. P. Bean, J. C. Fisher, and D. A. Vermilyea, *Phys. Rev.* **101** (1956) 551.
19. C-Y. Chao, L. F. Lin, and D. D. Mac Donald, *J. Electrochem. Soc.* **128** (1981) 1187.
20. M. Bojinov, I. Kanazirsky, and A. Girginov, *Electrochim. Acta* **41** (1996) 2695.
21. M. Volmer, *Phys. Z.* **22** (1921) 646.
22. W. Kossel, *Nachr. Ges. Wiss.* (1927) 135.
23. I. Stranski, *Z. Phys. Chem.* **136** (1928) 259.
24. T. Erdey-Grúz and M. Volmer, *Z. Phys. Chem.* **A159** (1931) 182.
25. M. Fleischmann and H. R. Thirsk, in *Advances in Electrochemistry and Electrochemical Engineering* (P. Delahay, C. W. Tobias, Eds.), Interscience: New York (1963), Vol. 3, Chapter 3.
26. M. Fleischmann and H. R. Thirsk, *Electrochim. Acta* **1** (1959) 146.
27. M. Fleischmann and H. R. Thirsk, *Electrochim. Acta* **2** (1960) 22.
28. A. Bewick, M. Fleischmann, and H. R. Thirsk, *Trans. Faraday Soc.* **58** (1962) 2200.
29. M. Avrami, *J. Chem. Phys.* **9** (1941) 177.
30. D. J. Astley, J. A. Harrisson, and H. R. Thirsk, *Trans. Faraday Soc.* **64** (1968) 192.
31. G. J. Hills, D. J. Schiffrin, and J. Thompson, *Electrochim. Acta* **19** (1974) 657.
32. J. W. M. Jacobs, *J. Electroanal. Chem.* **247** (1988) 135.
33. B. R. Scharifker, *J. Electroanal. Chem.* **240** (1988) 61.
34. R. G. Barradas and E. Bosco, *Electrochim. Acta* **31** (1986) 949.
35. S. K. Rangarajan, *Faraday Symp. Chem. Soc.* **12** (1977) 101.
36. H. Angerstein Kozlowska, B. E. Conway, and J. Klinger, *J. Electroanal. Chem.* **87** (1978) 301.
37. E. Bosco and S. K. Rangarajan, *J. Chem. Soc. Faraday Trans.* **77** (1981) 483.
38. E. Bosco and S. K. Rangarajan, *J. Electroanal. Chem.* **129** (1981) 25.
39. M. Noel, S. Chandrasekaran, and C. Ahmed Basha, *J. Electroanal. Chem.* **225** (1987) 93.
40. J. Wojtowicz, N. Marincić, and B. E. Conway, *J. Chem. Phys.* **48** (1968) 4333.
41. K. Ogura, *Electrochim. Acta* **25** (1980) 335.
42. U. Ebersbach, K. Schwabe, and K. Ritter, *Electrochim. Acta* **12** (1967) 927.
43. W. J. Müller, *Trans. Faraday Soc.* **27** (1931) 737.
44. A. J. Calandra, N. R. Tacconi, R. Pereiro, and A. J. Arvia, *Electrochim. Acta* **19** (1974) 901.
45. D. D. Mac Donald, *Transient Techniques in Electrochemistry*, Plenum Press: New York (1977), Chapter 8.
46. D. Devilliers, F. Lantelme, and M. Chemla, *Electrochim. Acta* **31** (1986) 1235.
47. S. Srinivasan and E. Gileadi, *Electrochim. Acta* **11** (1966) 321.
48. B. E. Conway, E. Gileadi, and M. Dzieciuch, *Electrochim. Acta* **8** (1963) 143.
49. H. Angerstein-Kozlowska, J. Klinger, and B. E. Conway, *J. Electroanal. Chem.* **75** (1977) 45 and 61.
50. A. Bewick and B. Thomas, *J. Electroanal. Chem.* **85** (1977) 329.
51. H. Angerstein-Kozlowska, J. Klinger, and B. E. Conway, *J. Electroanal. Chem.* **95** (1979) 1.
52. A. Sadkowski, *J. Electroanal. Chem.* **97** (1979) 283.
53. H. Angerstein-Kozlowska and B. E. Conway, *J. Electroanal. Chem.* **113** (1980) 63.
54. E. Bosco and S. K. Rangarajan, *J. Chem. Soc. Faraday Trans.* **77** (1981) 1673.
55. S. A. Arulraj and M. Noel, *Electrochim. Acta* **33** (1988) 979.
56. G. A. Mabbott, *J. Chem. Educ.* **60** (1983) 697.
57. P. T. Kissinger and W. R. Heineman, *J. Chem. Educ.* **60** (1983) 702.
58. D. H. Evans, K. M. O'Connell, R. A. Petersen, and M. J. Kelly, *J. Chem. Educ.* **60** (1983) 290.
59. T. F. Sharpe and S. G. Meibhur, *J. Chem. Educ.* **46** (1969) 103.
60. F. G. Will, *J. Electrochem. Soc.* **133** (1986) 454.

61. B. F. Giannetti, P. T. A. Sumodjo, and T. Rabockay, *J. Appl. Electrochem.* **20** (1990) 672.
62. B. F. Giannetti, P. T. A. Sumodjo, T. Rabockay, A. M. Souza, and J. Barbosa, *Electrochim. Acta* **37** (1992) 143.
63. B. F. Giannetti and T. Rabockay, *J. Braz. Chem. Soc.* **4** (1993) 61.
64. C. M. V. B. Almeida and B. F. Giannetti, *Mat. Phys. Chem.* **69** (2001) 261.
65. C. M. V. B. Almeida, B. F. Giannetti, and T. Rabóczkay, *J. Electroanal. Chem.* **29** (1999) 123.
66. Y. M. Chen, T. J. O'Keefe, and J. James, *Thin Solid Films* **129** (1985) 205.
67. V. Tsakova and A. Milchev, *J. Electroanal. Chem.* **253** (1987) 237.